Hydration Layer Coupling and Cooperativity in Phase Behavior of Stimulus Responsive Peptide Polymers

Dennis Kurzbach,[†] Wafa Hassouneh,[‡] Jonathan R. McDaniel,[‡] Eva A. Jaumann,[†] Ashutosh Chilkoti,[‡] and Dariush Hinderberger*,[†]

[†]Max Planck Institute for Polymer Research, Ackermannweg 10, 55128 Mainz, Germany

[‡]Department of Biomedical Engineering, Duke University, 136 Hudson Hall, Box 90281, Durham, North Carolina 27708-0281, United States

Ⓢ Supporting Information

ABSTRACT: It is shown that hydrophilic (backbone) and hydrophobic (side chain) hydration layers of elastin-like polypeptides (ELPs), a class of stimulus responsive peptide polymers that exhibit lower critical solution temperature (LCST) phase transition behavior, can exist in a coupled and decoupled state. The decoupled hydration state consists of hydrophobic and hydrophilic hydration layers that respond independently to temperature, while the coupled hydration

state is characterized by a common, cooperative dehydration of both hydration layers. It is further shown that the primary sequence of an ELP can be tuned to exhibit either of the hydration layer coupling modes. Charged side chains lead to decoupling, while strongly hydrophobic side chains trigger stronger interaction between hydrophilic and hydrophobic hydration, leading to coupling of both layers. Further, for aprotic residues this coupling is fostered by decreasing bulkiness of hydrophobic side chains due to larger hydration numbers and water molecules mediating coupling between side chain and backbone hydration shells. For coupled hydration shells, the LCST phase transition characterized by spin probing continuous wave electron paramagnetic resonance spectroscopy is reminiscent of a first-order process even on nanoscopic length scales. In contrast, analogous synthetic polymers exhibit nanoscale phase transitions over a broad temperature range, indicating that their nanoscale phase behavior is not of first order. Hence, our results indicate that ELPs are the first identified class of polymers that exhibit a first-order inverse phase transition on nanoscopic length scales. These results may also provide insights into the role of hydration layers in governing the structure−function relationship of intrinsically disordered proteins.
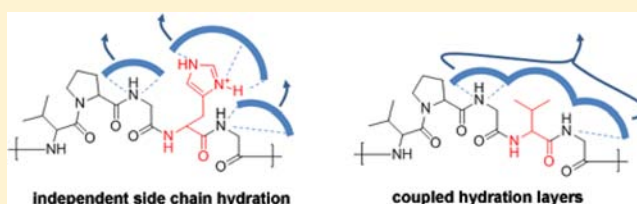
■ INTRODUCTION

The first suggestion of coil-to-globule transitions in responsive polymers that exhibit lower critical solution temperature (LCST) phase behavior appeared in 1960.[1] Although LCST phase behavior has, since this first report, been seen in many synthetic polymers in different solvents,[2,3] LCST polymers that display this behavior in water are of particular importance because of the broad interest in their applications in protein purification,[4,5] drug delivery,[6−9] tissue engineering,[10] immunoassays,[11] and molecular actuation.[12] Hence, understanding the molecular determinants that drive the phase behavior of this class of LCST polymers is critical for their rational design.

Despite the enormous literature on LCST behavior of polymers in water,[13] the underlying molecular origins remain elusive mainly for two reasons: First water itself is an anomalous solvent whose fundamental properties are still not completely understood.[14] The second and related reason is that the LCST phase behavior in water is driven by changes in the molecular conformation and hydration state of LCST polymers as a complicated function of solution conditions, such as temperature or salt concentration.[15,16]

Driven by the goal of understanding the molecular details of the LCST transition of polymers as a function of key molecular

parameters, i.e., chain length, sequence and composition, we focused our attention on a class of LCST peptide polymers called elastin-like polypeptides (ELPs) that exhibit LCST phase behavior in aqueous solvents.[17−19] ELPs are genetically encoded polymers composed of repeats of the amino acid VPGXG motif found in tropoelastin (X being any amino acid except P), and their LCST phase behavior can be precisely tuned at the molecular level by the choice of the guest residue, X, their chain length, and by cosolutes.[20,21] Due to the limited number of available techniques to study these unstructured and noncrystallizable biological macromolecules, linking the molecular properties of ELPs—and other LCST polymers—with their ensemble behavior remains a great challenge. For example, studying the solution conformation of ELPs using NMR is difficult because of the broad resonances that arise from the highly repetitive ELP sequence and hindered residue dynamics above the LCST.[22−25] Circular dichroism (CD) spectroscopy remains the method of choice,[16,26] but it provides limited structural information on the ELP and none about the role of solvation.

We chose ELPs as a model polymer system to study LCST phase behavior, because unlike synthetic LCST polymers, they can be genetically encoded so that their sequence, stereochemistry, and chain length can be precisely specified. Because chain length and composition impact their LCST behavior,[21] we hypothesized that the precise relationship between polymer sequence and chain length and hydration and its consequence on LCST behavior could be elucidated by the study of ELPs. This relation would be much more difficult to study for synthetic LCST polymers, whose sequence, chain length, and polydispersity are far more difficult to systematically control.[3] Understanding the LCST phase transition of ELPs is also of interest as they provide a simple model system that recapitulates aspects of the biophysical behavior of intrinsically disordered proteins (IDPs) that have recently attracted much attention.[27−30]

We chose continuous wave (CW) electron paramagnetic resonance (EPR) spectroscopy as spectroscopic method because of its favorable time and length scale[3] to study the molecular details of the solvation of ELPs as a function of temperature. CW EPR is an underutilized but powerful spectroscopic method that can report the polarity and hydrophilicity/hydrophobicity in complex aggregates of soft matter systems (like collapsed LCST polymers) on a nanoscopic length scale.[3] Although CW EPR offers a potent and simple methodology to examine the solvation of polymers, it has only been used to study ELPs in one previous study. Covalent conjugation of an EPR-active nitroxide spin label to an ELP was employed with the goal of using this conjugate as a "molecular thermometer" to monitor mild clinical hyperthermia in vivo.[31] CW EPR has been used to investigate synthetic stimuli responsive polymers,[32−36] but the results of these studies were confounded by the general structural inhomogeneity and polydispersity of chemically synthesized polymers. As we show, the molecular weight (MW) plays an important and unexpected role in controlling temperature-dependent solvation of LCST polymers, that is only revealed by the study of perfectly monodisperse polymers with a range of MWs, as it is made possible by the genetically encoded ELPs used here.

The results of this present study are both striking and unexpected. First, we show that hydrophilic and hydrophobic hydration layers in ELPs can exist in either a coupled or a decoupled state. The decoupled state denotes individual temperature-dependent dehydration of the two types of hydration layers found in ELPs, while the coupled state is characterized by a common, cooperative phase transition of both layers. Second, we demonstrate that the primary sequence of an ELP controls the coupling mode. The coupling between hydration shells significantly influences the molecular phase behavior of ELPs.

RESULTS AND DISCUSSION

We first systematically studied the effect of two orthogonal molecular parameters on the LCST phase behavior of ELPs: (1) the guest residue composition (X in the VPGXG repeat motif), which was varied from 100% alanine (most hydrophilic) to 100% valine (most hydrophobic); and (2) the chain length, which was varied between 40 and 120 pentapeptides. Building upon these results, we then investigated the effect of ionizable side chains, introduced through periodic lysine or histidine residues in the ELP at the guest residue position, X, on their LCST transition behavior. The ELPs in this study are denoted as X-Y, where X is the guest residue composition in the

VPGXG repeat unit (e.g., V_8A_2 denotes an ELP with 80% of the guest residues being valine and 20% alanine) and Y is the number of pentapeptide repeats (cf. Table 1; for the exact amino acid sequence of all ELPs, see the Supporting Information).

Table 1. Summary of Properties of ELPs: Composition and Corresponding LCST

	A-40[b]	A_8V_2-40[b]	A_5V_5-40	A_2V_8-40	V-40
composition[a]	100% A	80% A/ 20% V	50% A/ 50% V	20% A/ 80% V	100% V
$T_{c,EPR}$, °C[c]	–	70 ± 1	52 ± 1	44 ± 1	38 ± 1
$T_{c,turbidimetry}$, °C	69.2	60.4	49.7	40.8	34.4
	A-80	A_8V_2-80	A_5V_5-80	A_2V_8-80	V-80
composition	100% A	80% A/ 20% V	50% A/ 50% V	20% A/ 80% V	100% V
$T_{c,EPR}$, °C	70 ± 1	54 ± 1	36 ± 1	34 ± 1	32 ± 1
$T_{c,turbidimetry}$, °C	66.4	52.8	41.1	32.9	28.1

[a]Composition denotes the composition of the guest residues Xaa, in the otherwise always identical Val-Pro-Gly-Xaa-Gly sequence. [b]The discrepancy between $T_{c,EPR}$ and T_c for ELP A/A_8V_2-40 is a consequence of large amounts of residual water in the ELP aggregates above the LCST, which screen the hydrophobic interaction between 16-DSA and the ELP aggregates. Such interactions between 16-DSA and A-y ELPs can only be observed at temperatures significantly above the LCST, since increased dehydration of the ELPs is needed for significant interaction between 16-DSA and the aggregates. [c]Note that $T_{c,EPR}$ denotes the onset of observable interaction between the ELP and 16-DSA, while T_c denotes the cloud point of the solution (i.e., the temperature of the inflection point in a turbidity profile).

SIDE CHAIN HYDROPHOBICITY AND BACKBONE CHAIN LENGTH AFFECT THE COOPERATIVITY OF THE INVERSE PHASE TRANSITION

We used CW EPR to study temperature-dependent changes in the hydration of ELPs by spectroscopically monitoring the physical interaction between the spin-labeled fatty acid 16-DSA (16-4,4-dimethyl-oxazolidine-N-oxyl stearic acid; Figure 1) and ELPs of different compositions in aqueous solution as a function of temperature. We chose 16-DSA as the EPR probe, as its octanol/water-partition coefficient clearly indicates a
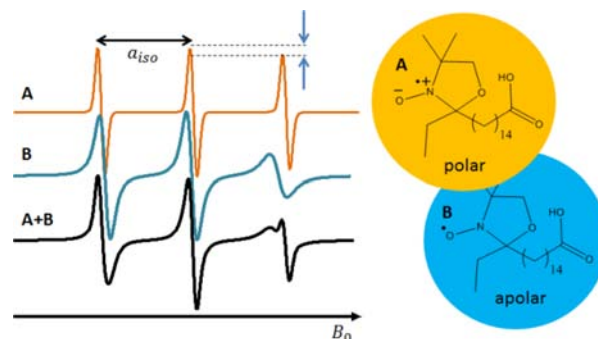

Figure 1. Environmental sensitivity of a 16-DSA CW EPR spectrum: 16-DSA in a polar environment (A; orange); 16-DSA in an apolar environment (B; blue); combined, bimodal spectrum (A+B; black). The dashed lines mark the difference in intensity between the central line of 16-DSA and the high-field transitions (right), which are dependent on τ_c. The value a_{iso} approximately corresponds to the separation of the zero crossings of two lines of a fast motion 16-DSA CW EPR spectrum.
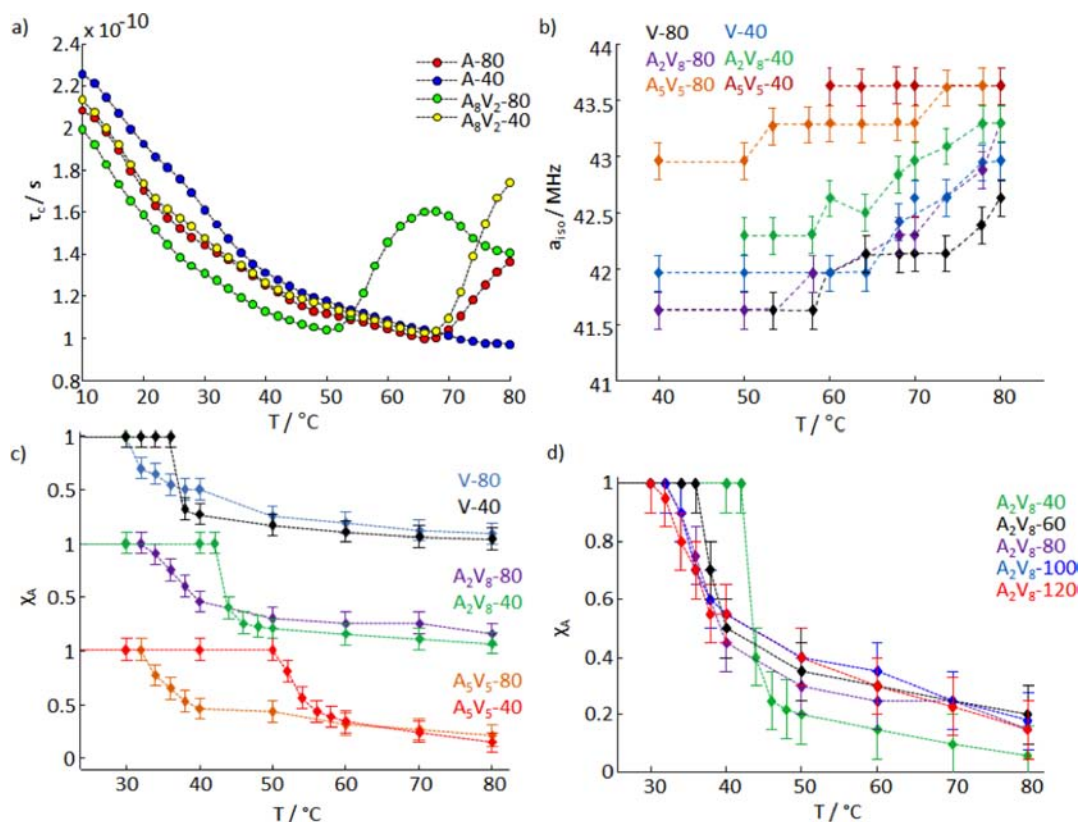
Figure 2. (a) Temperature dependence of τ_c for ELPs A-*y* and A_8V_2-*y*. (b) The Temperature dependence of the isotropic hyperfine-coupling constant (a_{iso}) of the DSA species B for selected two-component spectra. The concentration of the ELPs was 1 wt % in all cases, and the DSA concentration was 1 mM. (c) Fraction of the DSA species A, χ_A, as a function of temperature for selected two-component spectra for ELPs of varying chain length and hydrophobicity. Error bars stem from uncertainties in the simulations. (d) Fraction of the DSA species A, χ_A, as a function of temperature for selected two-component spectra for ELP A_2V_8 with varying chain length. Note that the fraction of incorporated spin probes only depends on the organic mass the ELPs provide for interaction with the probes. Therefore, all measurements were performed at 1 wt % ELP concentration. Note that some data points have been omitted for clarity.

strong preference for apolar environments $(\log(P)_{octanol/water} = 4.49).^{37}$ The rationale behind our approach is that 16-DSA is likely to interact strongly with desolvated aggregates of ELPs above their LCST. We also performed a scouting study using a frequently used more hydrophilic probe, 2,2,6,6-tetramethylpiperidin-1-yl)oxyl[3] (TEMPO), but as it does not show significant interactions with ELPs due to diminishing hydrophobic attraction, we did not use it further (see the Figure S6). The ELP concentration was 1 wt %, and the 16-DSA concentration was 1 mM in all the experiments reported herein.

Figure 1 shows that one can discern the spectral components of 16-DSA in a polar, water-rich environment (denoted species A; orange) from 16-DSA embedded in a nonpolar environment provided by a dehydrated (water-depleted) ELP aggregate above the LCST (denoted species B; blue). This is true even in the combined, bimodal spectrum (A+B; black). However, 16-DSA in the presence of aggregated ELPs can also exhibit a single-component spectrum (averaged between A and B). If the residence time of probes inside ELP aggregates is short (on the EPR time scale of $\sim 10^{-5}-10^{-9}$ s),^{35} one observes a single averaged high-field line. Only if the probes interact quite strongly with the host structure and residence times are longer than the above time scale, one observes a bimodal spectrum and two discernible high-field lines (superposition of A+B). Such a two-site situation with two well-separated lines is only observable if the relation $\tau_B^{-1} \ll \Delta\omega$ holds, where $\Delta\omega$ denotes the spectral line separation and τ_B the residence time of 16-

DSA in an ELP aggregate.^{35} In contrast, if $\tau_B^{-1} \gg \Delta\omega$, one observes a single line averaged between species A and B. For a single-component spectrum, the rotational correlation time of an "average" probe, τ_c, is the relevant parameter to characterize the LCST phase transition, as it reports on the average rotational freedom of a 16-DSA probe. Increasing τ_c is indicative of steric confinement as a result of ELP aggregation. For two-component spectra, the spectral contribution of 16-DSA strongly interacting (χ_B) or noninteracting ($\chi_A = 1 - \chi_B$) with ELP aggregates is more suitable for the characterization of the LCST phase transition, because the τ_cs of the separated spectral component A and B are not significantly affected by this transition. In such a case, the spectral component B appears at the LCST of the ELPs. To distinguish the phase transition observed by EPR from the macroscopic cloud point observed by turbidimetry, we denote cloud-point-derived collapse temperatures as $T_{c,turbidimetry}$ and the EPR-derived collapse temperatures as $T_{c,EPR}$. The isotropic hyperfine coupling constant, a_{iso}, which is approximately the spectral separation of the zero crossings in the CW EPR spectra is the third important spectroscopic parameter, as a decreasing a_{iso} reports a lowered polarity of a probes' local environment (see Figure 1). Note that in the case of ensemble averaging, a decrease in a_{iso} corresponds to transient incorporation of 16-DSA into water-depleted regions of a system and is hence indicative of the LCST transition of ELP solutions. For a distinct spectral component B that appears at the LCST, a_{iso} is initially small,

and further changes in a_{iso} do not correspond to the initial aggregation of the ELPs but rather to subsequent processes. The values a_{iso} and τ_c were both extracted from rigorous spectral simulations, details of which are reported in the methods section of the Supporting Information. Note that we only quantify spectral contributions of strongly interacting probes through χ_B. The fraction of 16-DSA probes incorporated in ELP aggregates might, however, be larger than χ_B if the probes reside in patches of intercalated water inside an aggregate, for example. However, ELP aggregates are typically assumed to be quite well-ordered,[38] such that χ_B is likely to at least approximately reflect the actual fraction of incorporated probes. The spectral contribution of species B furthermore exactly corresponds to the fraction of strongly interacting probes. This holds independent of probe site-exchange frequencies as long as the two spectral components are clearly discernible.[35]

Figure 2 shows all three parameters, τ_c (2a), a_{iso} (2b), and χ_A (2c,d) for a set of ELPs with composition A_x-V_{10-x}-y (from A-y, most hydrophilic, to V-y, most hydrophobic) as a function of temperature; the experimental data and respective analyses that yields these plots are contained in the Supporting Information (see methods and experimental sections and Figures S1−S5). For the most hydrophilic ELPs with high alanine content (A/A_8V_2-y with 80−100% of the guest residues being alanine; see Table 1 and Figure 2) we observe a single high-field line above the LCST in the CW EPR spectra (Figures 2a and S1). Yet, that there is contact between 16-DSA, and aggregates of these ELPs can be deduced from the rotational mobility of 16-DSA probes, which decreases with higher temperature, corresponding to an increasing τ_c. This observation, in combination with the presence of a single-component spectrum, indicates a short-lived and weak, though significant, interaction between 16-DSA and the hydrophilic ELPs A/A_8V_2-y (see Figures 2a and S1 and Table 1 for $T_{c,turbidimetry}$ and $T_{c,EPR}$ values). In contrast, for the more hydrophobic ELPs with a valine content ≥50%, we observe two clearly separated high-field lines above the LCST (see Figure S1) with a probe species lifetime (i.e., residence time in the ELPs) of $\Delta\omega \approx 3.5$ MHz → $\tau_B > 0.3$ μs. Hence, one can unequivocally state that with increasing hydrophobicity of the ELP, the residence time of 16-DSA in the ELP aggregates above the LCST becomes longer.

The different residence times of 16-DSA in ELP aggregates of varying hydrophobicity can be rationalized as follows: With increasing ELP hydrophilicity and length, the polarity that the probes sense in an aggregate increases because of an increase in the number of water molecules surrounding the probe within the ELP aggregate. The presence of water in the proximity of the probes screens any attractive hydrophobic interactions between the probes and the ELPs, which consequently leads to shorter species B lifetimes (see Figure 3).

The varying amounts of water sensed by 16-DSA in aggregates of different ELPs can be deduced from Figure 2b, where a_{iso} of species B for ELPs A_5V_5/A_2V_8/V-y-y is plotted as a function of temperature. With increasing ELP length and hydrophobicity, a_{iso} becomes smaller at a given temperature, meaning that the probes experience a lower environmental polarity. This is clearly observable between 40 and 50 °C, where a_{iso} remains constant for a given ELP as the probe-exchange frequency does not significantly change in this temperature regime. The parameter a_{iso} of species B increases with temperature for ELPs A_5V_5/A_2V_8/V-y (Figure 2b), which is a consequence of increasing probe-site exchange frequencies
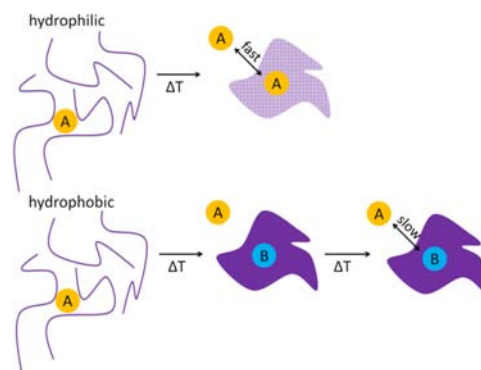

Figure 3. Sketch of the ELP-16-DSA interaction. A and B denote 16-DSA species corresponding to the spectral components A and B. For more hydrophilic ELPs above the LCST, the DSA probes can quickly exchange between ELP-rich and -depleted regions. For more hydrophobic ELPs, DSA probes do not exchange at temperatures slightly above the LCST. At even greater temperatures, the probes start to exchange slowly.

between ELP aggregates and solvent within the regime of slow exchange[35] due to increasing diffusional displacement with temperature (see Figure 3).[3] Hence, in aggregates of longer and more hydrophobic ELPs, the probes sense less water in their immediate vicinity (probably through residual backbone- or side-chain hydration) than in shorter and more hydrophilic ELP aggregates. This deduction is further corroborated by the $T_{c,turbidimetry}$s and $T_{c,EPR}$s, which indicate decreasing stability of bound hydration shells with increasing main chain length and side chain hydrophobicity (see Table 1).

This finding suggests that the molecular/nanoscale properties of different ELPs are dissimilar above their LCST. Depending on the primary sequence and length, ELP aggregates above the LCST have significantly different polymer densities. This gives rise to different modes of host−guest interactions, despite the fact that the ELPs nominally appear to undergo a similar phase transition at the macroscopic level, as observed by the change in solution turbidity at their LCST.[39]

It should be noted that compared to other synthetic thermoresponsive polymers, the spin probes generally sense larger amounts of residual water in aggregates of ELPs above the LCST. This suggests that on average, aggregates of ELPs retain significantly more water than synthetic LCST polymers that have been investigated by CW EPR, likely due to the polar nature of amino acids, as compared to typical synthetic monomers.[33,34,36] For 16-DSA, the observed hyperfine couplings (see Figure 2b, 41.5 MHz < a_{iso} < 44 MHz) consistently indicate a polarity that is similar to that found in mixtures of isopropanol and chloroform ($a_{iso,i\text{-propanol}}$ = 44.2 MHz to $a_{iso,chloroform}$ = 41.4 MHz). In contrast, the polarity of apolar cavities of thermoresponsive synthetic polymers typically leads to $a_{iso} < 41.5$ MHz. For comparison, a_{iso} in aqueous solution is 44.6 MHz.[3,33,40]

COOPERATIVITY OF THE INVERSE PHASE TRANSITION

The sequence- and length-dependent strength of ELP hydration leads to tunable host−guest interaction and to some extent different phase behavior compared to synthetic LCST-exhibiting polymers. For synthetic LCST polymers, one often observes that the onset of the phase transition (proceeding via local collapse and nanoscale inhomogeneities),[3]

detectable by spin probing CW EPR, is located at lower temperatures than the macroscopic LCST typically detected by methods like turbidimetry.[34] In contrast, we observe that the macroscopic LCST[21,39] of ELPs, $T_{c,turbidimetry}$, generally coincides with the onset of nanoscopic collapse, $T_{c,EPR}$ (see Table 1). Taking into account that for ELPs $A_5V_5/A_2V_8/V$-y the fraction of 16-DSA interacting with an ELP is quite prominent already a few degrees above $T_{c,EPR}$, one can rule out that the cloud point is just a consequence of sparse physical interactions between ELPs leading to cross-linking between ELP molecules. Thus, the ELP-phase transition does not proceed via local collapse and subsequent percolation or related mechanisms[3] but instead proceeds by cooperative aggregation of ELP chains. In light of recent studies on nanoscale properties of thermoresponsive soft matter[3,40] this cooperative aggregation is surprising. The temperature dependence of the spectral contribution of residual free 16-DSA (χ_A) in Figure 2c,d further illustrates that the phase transition is sharp for the 40 pentamer ELPs (for details on the χ_A calculation see the Methods section of the Supporting Information). The respective transitions for the longer ELPs with 80 or more pentamers are significantly broader. This latter behavior is similar to the behavior of synthetic LCST polymers, for which the macroscopic (often sharp) transition observed by temperature-dependent turbidimetry is accompanied by a steady dehydration process that proceeds over a wide temperature range (typically ~40 K).[32−34,36]

In contrast, the χ_A temperature profiles for x-40 (and to some extent also x-60) ELPs show a very steep and even sigmoidal development in a very narrow temperature range (2−3 K) that is indicative of a cooperative process. This suggests that the dehydration-induced aggregation of these short ELPs at the LCST is a highly cooperative process even on the nanoscopic length scale probed by EPR. The cooperative dehydration of ELPs has been previously proposed by Cremer and co-workers.[20] They suggested that the hydrophilic hydration shell of the backbone of the ELPs, and the hydrophobic hydration shell of the amino acid side chains might exist in a coupled state, leading to a cooperative dehydration process. Note that our samples were allowed to equilibrate for 10 min after each temperature step of 2 K and that during this interval no changes in the spectra were observed. Hence, it is safe to state that slow kinetics do not affect the observed phase transition.

To further analyze these results, we assumed the spectral fraction χ_A at 80 °C as a reference for the fraction of aggregated ELPs, since χ_A is identical for all ELPs under investigation at this temperature (within the error bounds). Using this reference, one can state that over 50% of the mass of ELPs V/A_2V_8-40 collapses and interacts with 16-DSA in a range of less than 5 °C. To the best of our knowledge, this is the most rapid inverse phase transition so far observed on nanoscopic length scales (seen by CW EPR). This in itself is an interesting finding, as this thermal response may possibly be regarded as a nanoscale first-order phase transition, while we previously found nearly exclusively broad and nonfirst-order phase transitions by CW EPR spectroscopy.[40]

Interestingly, the impact of chain length on the cooperativity (sigmoidality) of the inverse phase transition increases with rising mean hydrophobicity of the guest residue, as can be observed in Figure 2c. For ELP V-y the transition is very sharp and sigmoidal for the 40 pentapeptide chain length, while it is broadened and does not show a sigmoidal temperature dependence for 80 pentapeptide long ELPs. In contrast, for

ELP A_5V_5-y there is no substantial effect of the chain length on the sharpness of the phase transition. This indicates that for more hydrophilic guest residues, the coupling between hydrophilic and hydrophic hydration layers is not influenced by the chain length. This is a consequence of more tightly bound water in the vicinity of more hydrophilic ELPs mediating the two types of hydration. In contrast, this mediating water is obviously absent in the case of more hydrophobic ELPs, so that hydration layer coupling is not observed in these systems. Consequently the effect of chain length on the width of the thermal transition is also not seen in hydrophobic ELPs (cf. Figure 2b and a_{iso} values). Hence, with varying chain length, subtle changes are seen in the coupling modes between hydrophilic and hydrophobic hydration.

This shows that the precisely tunable molecular length of ELPs controls the nanoscale phase transition order, as observed by CW EPR. The sharp, first-order nanoscale transition exhibited by the short ELP (40 pentapeptides) may be attributed to a stronger coupling between hydrophilic and hydrophobic hydration shells for short ELPs as compared to longer ELPs, which exhibit second or nonorder transitions. The fact that shorter ELPs are more strongly hydrated than longer ones is reflected in their $T_{c,turbidimetry}$s and $T_{c,EPR}$s as well as in the amounts of residual hydration after aggregation (see Figure 2b). This stronger hydration, in turn, may mediate the coupling between the different hydration types.[15,20] The energetic reason for the proposed difference in hydration layer coupling between the shorter 40/60 pentapeptides long ELPs and the longer 80 or more pentapeptides long ELPs is the increasing loss in entropy due to hydration of the ELP with growing chain length.[14,41] Hence, longer ELPs are less strongly hydrated than the shorter ones. Fewer water molecules per pentapeptide repeat hydrate them, which might mediate the coupling between the two hydration layers. Thus, in longer ELPs coupling between hydration layers, reflected in sharp phase transition events, is not observed.

The assumption of coupling of hydration shells can further account for the fact that the dehydration process starts at lower temperatures for the longer ELPs, while the dehydration process, once started, is much sharper for the shorter ones. If hydrophobic and hydrophilic hydration shells are not as strongly coupled in longer ELPs, less energy is needed to initiate the dehydration, since weak coupling may allow for independent dehydration of the two types of hydration shells. Note that one does not typically observe any dependencies of $T_{c,EPR}$s on chain length or concentration in synthetic polymers, since one exclusively monitors the local conformation of the chains with CW EPR.[34,36] This furthermore corroborates the idea that ELPs initially aggregate without the formation of nanoscopic transition structures, as such aggregation processes are dependent on the chain length.[39] It should be noted that many common thermoresponsive systems are believed to initially aggregate at the LCST since investigations with macroscopic techniques point to that. However, detailed CW EPR analysis frequently reveal a heterogeneous ensemble of nanoscopic transition states, such as collapsed unimer globules or oligomers with a small and variable aggregation number, which can be the dominant species in a system over a wide temperature range.[3,33,34,40]

Based on the above results, we hypothesize that bound water molecules that mediate coupling between side chain and backbone hydration layers can consistently and entirely explain the differences in cooperativity and sharpness of the inverse
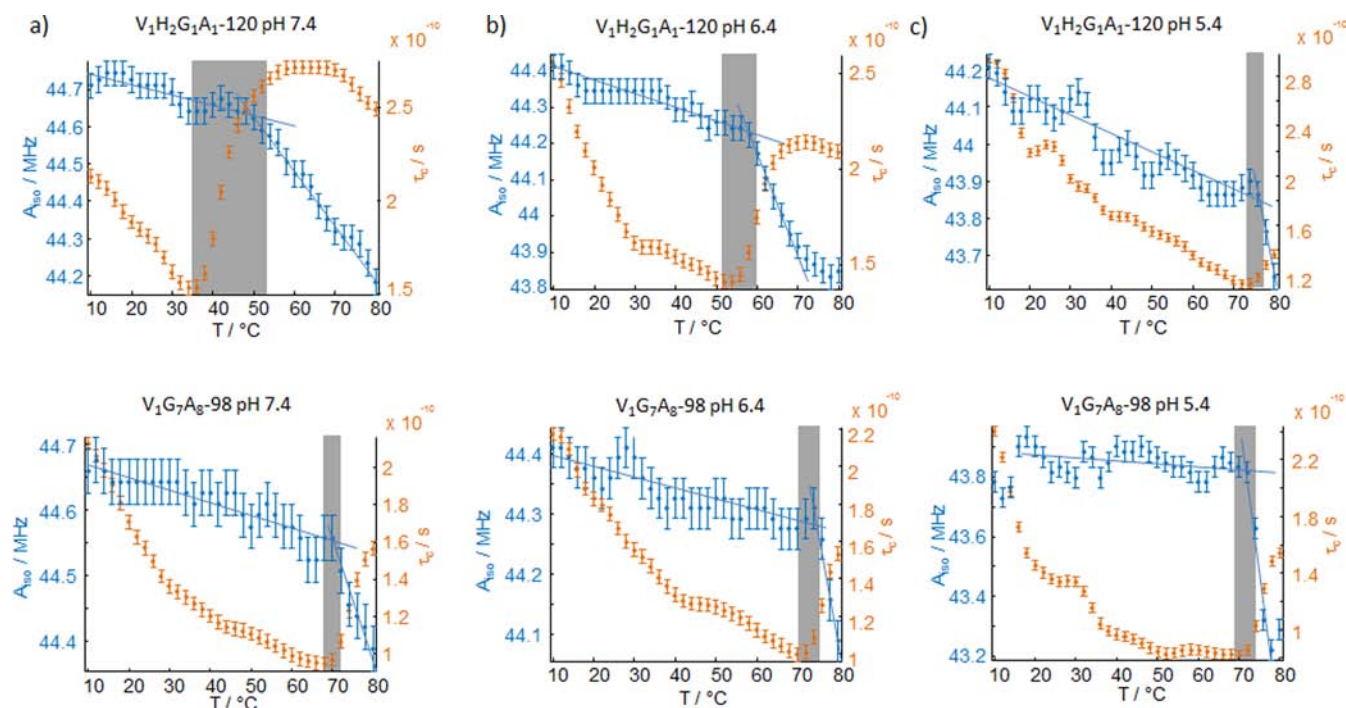
Figure 4. Temperature dependence of a_{iso} and τ_c for 16-DSA in presence of protic, histidine-containing ELP $V_1H_2G_1A_1$-120 and aprotic ELP $V_1G_7A_8$-98 at pH (a) 7.4, (b) 6.4, and (c) 5.4. The gray bars indicate the difference in $T_{c,1}$ and $T_{c,2}$.

phase transition of A_xV_{10-x}-y ELPs. In the following we will show with ionizable ELPs that this hydration layer coupling can directly be observed by means of spin probing CW EPR.

■ SIDE CHAIN POLARITY DETERMINES COUPLING BETWEEN HYDROPHOBIC AND HYDROPHILIC HYDRATION LAYERS

Figure 4 shows rotational correlation times and a_{iso} values for two ELPs: $V_1H_2G_1A_1$-120 and $V_1G_7A_8$-96. Note that Figure 4 shows a_{iso} values for fast site-exchanging 16-DSA probes. Hence, these values cannot directly be compared with the a_{iso} values shown in Figure 2b, which stem from an individual spectral component B in the limit of slow exchange. Data for $V_1H_2G_1A_1$-120 are representative for other histidine-containing ELPs. These ELPs can be ionized by setting the solution pH to values below the pK_a of the His side chains (pK_a(His) ≈ 6). For more related data on other histidine-rich ELPs see Figures S7, S8, and Table 2. The sharp increase in τ_c at ~32 °C and

Table 2. Observed Transition Temperatures for the Different ELPs under Investigation at pH 7.4[a]

	V_1H_4-80	$V_1H_2G_1A_1$-120	$V_1G_7A_8$-160	$V_1G_7A_8$-96
$T_{c,EPR1}$	32 °C	36 °C	64 °C	70 °C
$T_{c,EPR2}$	56 °C	48 °C	64 °C	70 °C

[a]$T_{c,EPR1}$ denotes the temperature of the first (τ_c) and $T_{c,EPR2}$ of the second (a_{iso}) observed transition. The concentration was 1 wt % in all cases.

physiological pH for $V_1H_2G_1A_1$-120 indicates the aggregation of the ELPs and the subsequent interaction with 16-DSA that affects the rotational mobility (compare Figure 2a). The τ_c-derived transition temperatures are listed in Table 2. In the following we denote the transition temperature observed through τ_c $T_{c,EPR-1}$. With decreasing pH and increasing degree

of protonation of histidine guest residues $T_{c,EPR-1}$ rises (histidine is primarily neutralized at pH 7.4 but nearly fully charged at pH 5.4). Interestingly, a second, independent phase transition can be observed via a_{iso} (indicating further dehydration of the ELPs) at temperatures above $T_{c,EPR-1}$. As seen in Figure 4, these transition temperatures observed via a_{iso} (denoted $T_{c,EPR-2}$ in the following) shift to higher temperatures with decreasing pH. At pH 5.4 $T_{c,EPR-2}$ even shifts into the region of $T_{c,EPR-1}$. Interestingly, for the nonionizable ELP, $V_1G_7A_8$-96 $T_{c,EPR-1} = T_{c,EPR-2}$. Most importantly $T_{c,EPR-2}$ is independent of the pH in this case. Note that independent of pH $T_{c,EPR-1} = T_{c,EPR-2}$ for any ELP with merely hydrophobic guest residues. The comparison between $V_1H_2G_1A_1$-120 and $V_1G_7A_8$-96 is hence representative for all histidine-rich and hydrophobic ELPs, respectively. All these observations can consistently be explained, when taking into account the two different types of hydration shells for the side chains and backbone. Since τ_c is sensitive to aggregation of ELPs, and dehydration of hydrophobic side chains is likely to trigger aggregation (even His has a quite extended organic scaffold), it appears reasonable to assume that $T_{c,EPR-1}$ is correlated to the temperature of side chain dehydration. The subsequent decrease in a_{iso} can in contrast be explained by a loss of hydrophilic hydration, correlating $T_{c,EPR-2}$ with less water in the direct (average) environment of the spin probes. Hence, $T_{c,EPR-1}$ and $T_{c,EPR-2}$ have to coincide if hydrophilic and hydrophobic hydration shells exist in a coupled state, and the two types of hydration layers vanish simultaneously. Yet, if $T_{c,EPR-1} \neq T_{c,EPR-2}$, the two hydration layers have to be decoupled. This latter scenario is observed for His-rich ELP $V_1H_2G_1A_1$-120 where $T_{c,EPR-2}$ depends on the pH and hence is different from $T_{c,EPR-1}$ (the same is true for V_1H_4-80; see Figure S8). In this case one observes a phase transition that can be regarded as a two-step process, during which hydrophobic hydration vanishes first, at lower temperatures than hydrophilic hydration (note that if

$T_{c,EPR-1} \neq T_{c,EPR-2}$ no significant changes in a_{iso} can be observed at $T_{c,EPR-1}$, indicating that the dehydrated side chains do not interact strongly with 16-DSA but more likely with each other in order to lead to aggregation). From the data in Figures 4 and S7 and S8 one can deduce that $T_{c,EPR1} \neq T_{c,EPR2}$ is only observable in the presence of ionizable side chains. We explain the difference between $T_{c,EPR-1}$ and $T_{c,EPR-2}$ in the presence of His by its proticity and its subsequent ability to form H-bonds with the solvent. It may therefore well be that His groups can stabilize a "hydrophobic" hydration shell on their own, independent of backbone hydration (Figure 5a), leading to
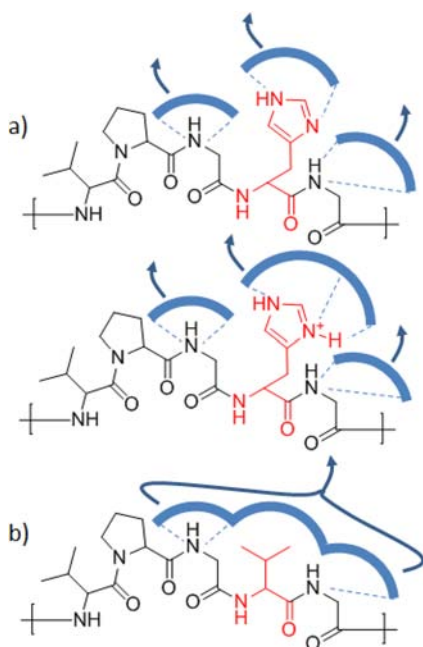

Figure 5. Sketch of the putative hydration for (a) ELPs with protic guest-residue side chains (red) and (b) with aprotic guest residue side chains (red). In (a) the hydration layer of the protic guest-residue side chain is individually stabilized by H-bonds and can vanish independently (decoupled) from backbone hydration layers. When the His residues are charged (a, bottom) the individual (decoupled) side chain hydration layers are even more stable than in the charge neutral analogue (a, top). The higher stability is schematically depicted as larger hydration shell and larger number of H-bonds. In (b) the hydration layer of the guest-residue side chain is stabilized via coupling to neighboring backbone hydration layers, and hence dehydration takes place cooperatively.

decoupling of the two types of hydration shells. Obviously ionization of the His side chains leads to a shift of $T_{c,EPR-2}$ to higher temperatures. This may likely be triggered by a stabilization of His solvation shells as a consequence of enhanced charge−dipole interactions between the imidazole and surrounding water and consequently more favorable solvation energies, since higher LCSTs typically are a consequence of more stable hydration shells. Likewise, this phenomenon may be explained by charged His resembling a more hydrophilic moiety, such that its hydration layer is of a hydrophilic nature itself, like the backbone hydration. This is in accordance with the fact that $T_{c,EPR-1}$ and $T_{c,EPR-2}$ are quite similar at pH 5.4, such hydrophilic backbone hydration and side chain hydration appear to have hydration shells of similar stability. Thus, with decreasing pH, i.e., increasing side chain mean charge, His residues are very likely to stabilize a hydration

shell on their own. This is schematically shown in Figure 5a. However, as $T_{c,EPR1} \neq T_{c,EPR2}$ even at pH 7.4 where His is largely unprotonated, it appears that even unprotonated His is already hydrophilic enough to stabilize an independent hydration layer on its own. In the absence of His, the hydrophobic hydration shells can likely only be stabilized through coupling to neighboring hydrophilic hydration shells as depicted in Figure 5b and as indicated by the pH independent equality of $T_{c,EPR-1}$ and $T_{c,EPR-2}$. This coupling would consequently lead to a single dehydration process at a temperature T_c (as observed for ELPs $V_1G_7A_8$-y and A_x-V_{10-x}-y with high A-content) since hydrophobic hydration would vanish together with the stabilizing hydrophilic hydration shell (Figure 5b), as in the case of charged His. Hence, for ELPs with a significant number of protic guest residues (capable of forming H-bonds with surrounding water molecules), the cooperativity of the thermal phase transition, the coupling between hydrophilic and hydrophobic hydration shells, respectively, is governed by the ability of the guest-residue side chains to stabilize a hydration shell on their own. Individual, decoupled hydration of side chains and backbone leads to a two-step inverse phase transition for which the two hydration shells vanish at different temperatures. In contrast, stabilization of hydrophobic hydration through neighboring hydrophilic hydration layers leads to a one-step inverse phase transition at T_c, as sketched in Figure 5. It is important to note that we did not observe any differences in the type of phase transition when the chain lengths/concentrations were varied for the ionizable ELPs (see the Figures S5 and S10). This is a consequence of the following: the local hydration and dehydration modes, i.e., coupled and decoupled backbone and side chain hydration layers, are dependent on the local H-bond network and amino acid sequence (cf. Figure 5). The global ELP concentration, however, does not affect the local H-bond patterns, since the primary sequence is not altered by changes in concentration. It is exactly this local, nanoscopic length scale for which CW EPR is strikingly sensitive (making our observations possible in the first place). Hence, the order and type (one- or two-step) of the phase transition observed on the nanoscale remains unaffected by the ELP concentration.

To support the conclusion that the coupling of hydration layers depends on the hydrophilicity of side chains, i.e., that protic side chains can stabilize individual, decoupled hydration layers, while completely hydrophobic and apolar side chains can only be hydrophobically hydrated through coupling to neighboring hydration layers, we additionally performed CW EPR experiments on an ELP containing valine and lysine in a ratio of 6:1 (ELP K_1V_6-56). This ELP was selected to investigate if the observed decoupling of hydration layers is just a special property of His-rich ELPs or a general consequence of hydrophilic guest residue side chains. At pH 9, lysine exists in a protonated and charged form, and at pH 11, it is primarily deprotonated and neutral (pK_a(Lys) ≈ 10.3). Thus, one would expect from the results on histidine-containing ELPs that side chain hydration layers are more unstable at pH 11 (neutral) but more stable at pH 9 (charged) for K_1V_6-56, since the stability of the side chain hydration layer is observed to increase with side chain charge. In extreme cases of very hydrophilic guest residue side chains, a coupling between hydration layers would only (if at all) take place at pH 11 (if the deprotonated guest residue side chains are quite hydrophobic and assuming a pK_a around 10), but decoupled hydration layers would occur only at pH 9. In Figure 6 one can
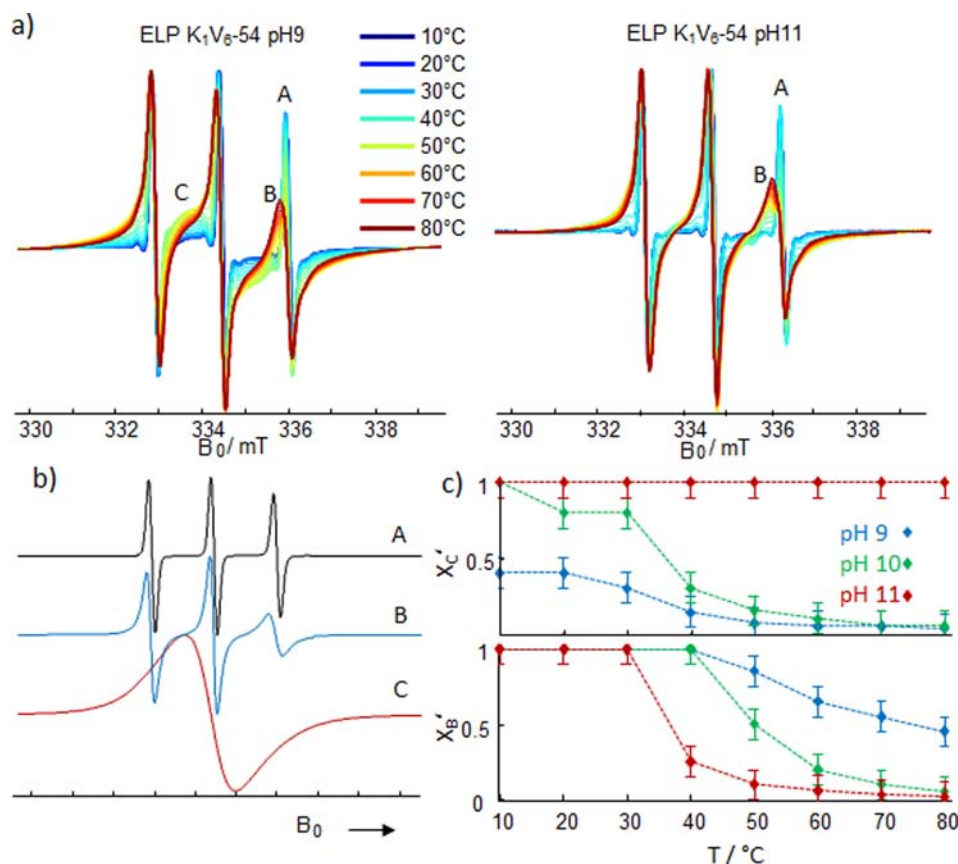
Figure 6. (a) Temperature dependence of CW EPR spectra of 16-DSA in solutions of ELPs K_1V_6-56 at pH 9 and 11. Spectral components are marked A, B and C. (b) Spectral components of spectra depicted in (a). (c) Relative spectral contribution of species B and C, as defined in (b) to the spectra depicted in (a) and in the Figure S7 (for pH 10). Note that spectral contributions are related to the axes via mole fractions $\chi_i = n_i/\sum n_j$. Thus, χ_B' and χ_C' denote the inverse contribution (cf. Figure 2c,d) of species B or C to the experimental spectra normalized to the other two components in each case.

observe that 16-DSA in solutions of K_1V_6-56 exhibits multicomponent spectra, as previously observed for the V_xA_{x-1}-Y ELPs with low A-content. The long residence time of 16-DSA incorporated into the ELP aggregates (evident from the bimodality of the CW EPR spectra above $T_{c,EPR}$), as compared to $V_1H_2G_1A_1$-120, is a consequence of the high valine content and the butyl moiety of lysine. Figure 6a shows the temperature dependence of the 16-DSA CW EPR spectra for K_1V_6-56. At pH 11 two spectral components A and B can be observed, similar to what has been described above for V_xA_{x-1}-Y (see Figures 1−3). At pH 9, however, one observes a third component C (see Figure 6b), which stems from an exchange broadened 16-DSA signal. The relative contributions of species B and C to the experimental CW EPR spectra at different temperature and pH are shown in Figure 6c. The observation that at pH 9, where lysine is charged, two distinct interaction modes of 16-DSA with K_1V_6-56 can be observed (through species B and C), but only one mode at pH 11 (species B) is in full agreement with the notion of strong decoupling between hydration shells due to charged side chains. At pH 9 species B and C appear separately as a consequence of individual lysine side chain hydration layers disintegrating at lower temperatures than backbone hydration. Thus, two types of packing modes arise for the ELP aggregates as a function of temperature giving rise to two different interaction modes with 16-DSA. At pH 11 both hydration layers are coupled, and only one species appears at a single collapse temperature. This is in agreement with the

fact that species B and C at pH 9 (and 10; see Figure S7) appear at different temperatures.

It should be mentioned that lysine, unlike histidine, seems not to be capable of stabilizing a hydration layer in its charge neutralized form. This is likely a consequence of the less polar nature of lysine side chains compared to histidine side chains. One observes decoupled hydration layers for lysine-rich ELPs only under acidic conditions. The more hydrophobic nature of lysine, when compared with histidine, makes charging of side chains obviously necessary to gain side chains that are hydrophilic enough to stabilize an individual, decoupled hydration layer.

Note that significantly lower lysine content (K:V = 1:16) does not lead to detectable contributions of species C, since only very few 16-DSA probes interact with charged lysine side chains in this case (see Figure S9 for the spectra). This information is important since one can exclude micellization effects of 16-DSA leading to species C and deduce that species C actually does arise from interaction with ELP K_1V_6-56. Importantly, our entire interpretation is supported by the fact that the phase transition of ELP K_1V_6-56 becomes more cooperative with increasing pH and stronger coupling of hydration layers (see Figure 6c). Also note that there are only few lysine residues present in the K_1V_6-56 ELP. However, since CW EPR is an intrinsically local experimental technique, it is not surprising that even this minor contributions to a given system can be observed as strong spectral contributions (B and

C). This is in agreement with our recent observation that even 2% of a hydrophobic comonomer in an otherwise hydrophilic poly(ethylene glycol) polymer is enough to lead to significant spectral contributions of hydrophobically sheltered spin probes in CW EPR. This is shown in detail in refs 3 and 34. Furthermore, the attractive electrostatic interaction between cationically charged lysine residues (and histidine) and deprotonated anionic 16-DSA might additionally foster the binding of 16-DSA to lysine side chains and such may increase the spectral contribution of species C, making species C more visible, although there are only few lysine residues in K_1V_6−56.

CONCLUSION

By self-assembly spin probing CW EPR spectroscopy we show herein that hydrophobic (side chains) and hydrophilic (backbone) hydration layers can exist in a coupled or decoupled state in ELPs. We show that the coupling between the two types of hydration layers significantly influences the phase behavior and cooperativity of the LCST transition of ELPs. Strong coupling leads to cooperative (even to first order) phase transitions on the nanoscale. Weak or no coupling leads to complex, two-step (second or non-order) transition mechanisms. Further, it is shown that the primary sequence of a polypeptide governs coupling modes between hydration layers. Charged side chains lead to decoupling, while strongly hydrophobic side chains trigger stronger interaction between hydrophilic and hydrophobic hydration. Aprotic, yet quite hydrophilic amino acids like glycine or alanine with only small (or missing) aliphatic side chains can also trigger hydration layer coupling because of increased numbers of hydrating water molecules, as compared to more hydrophobic residues. We show that this also leads to coupling between hydration layers, as more water in the vicinity of the polypeptide chain mediates coupling between the side chain and backbone hydration shells. ELPs as models substrates exhibit fully controllable molecular structure and highly repetitive sequences. Furthermore, CW EPR spectroscopy as an intrinsically local technique allows for elucidating phenomena beyond ensemble averaged and macroscopic standards.[3,40] These two facts in combination with the high environmental sensitivity of nitroxide spin probing CW EPR made the described observations possible. Finally, the observation of coupled and decoupled hydration layers is a useful concept that deserves further exploration to understand how hydration layers govern the structure−function relationship of intrinsically disordered proteins, and more broadly how the primary sequence of all proteins determines the constitution of their hydration shells. Because IDPs typically contain large amounts of charged residues,[28] our results insinuate that decoupled hydration layers may have implications for IDP function. Such decoupling may foster side chain dehydration processes that are essential in folding-upon-binding processes[30] and allow for low activation energies of fast structural transitions,[42] while aggregation due to dehydration of the protein is circumvented because of residual backbone hydration.

ASSOCIATED CONTENT

Ⓢ Supporting Information

Supplementary CW EPR data, experimental details, details on data analysis, and a description of the spin probing approach. This material is available free of charge via the Internet at http://pubs.acs.org.

AUTHOR INFORMATION

Corresponding Author

dariush.hinderberger@mpip-mainz.mpg.de

Notes

The authors declare no competing financial interest.

REFERENCES

(1) Stockmayer, W. H. *Makromol. Chem.* **1960**, *35*, 53.
(2) Winnik, F. M.; Ottaviani, M. F.; Boßmann, S. H.; Pan, W.; Garcia-Garibay, M.; Turro, N. J. *Macromolecules* **1993**, *26*, 4577.
(3) Kurzbach, D.; Junk, M. J.; Hinderberger, D. *Macromol. Rapid Commun.* **2013**, *34*, 119.
(4) Hassouneh, W.; Christensen, T.; Chilkoti, A. *Curr. Protoc. Prot. Sci.* **2010**, *6*, 11.1.
(5) Trabbic-Carlson, K.; Liu, L.; Kim, B.; Chilkoti, A. *Protein Sci.* **2004**, *13*, 3274.
(6) Marx, R. J.; Osborne, R. D.; Stevens, M. S.; Ulijn, R. V. *Soft Matter* **2006**, *2*, 822.
(7) McDaniel, J. R.; Callahan, D. J.; Chilkoti, A. *Adv. Drug Delivery Rev.* **2010**, *62*, 1456.
(8) MacEwan, S. R.; Callahan, D. J.; Chilkoti, A. *Nanomedicine* **2010**, *5*, 793.
(9) Chilkoti, A.; Dreher, M. R.; Meyer, D. E.; Raucher, D. *Adv. Drug Delivery Rev.* **2002**, *54*, 613.
(10) Nettles, D. L.; Chilkoti, A.; Setton, L. A. *Adv. Drug Delivery Rev.* **2010**, *62*, 1479.
(11) Kim, J.-Y.; O'Malley, S.; Mulchandani, A.; Chen, W. *Anal. Chem.* **2005**, *77*, 2318.
(12) Kim, B.; Chilkoti, A. *J. Am. Chem. Soc.* **2008**, *130*, 17867.
(13) Aseyev, V.; Tenhu, H.; Winnik, F. M. *Adv. Polym. Sci.* **2011**, *242*, 29.
(14) Israelachvili, J. N. *Intermolecular and Surface Forces*; Elsevier: London, 2011; Vol. 3.
(15) Castiglione-Morelli, A.; Scopa, A.; Tamburro, A. M.; Guantieri, V. *Int. J. Biol. Macromol.* **1990**, *12*, 363.
(16) Urry, D. W. *J. Protein Chem.* **1988**, *7*, 1.
(17) Rousseau, R.; Schreiner, E.; Kohlmeyer, A.; Marx, D. *Biophys. J.* **2004**, *86*, 1393.
(18) Li, B.; Alonso, D. O. V.; Dagett, V. *J. Mol. Biol.* **2001**, *205*, 581.
(19) Zhang, Y.; Trabbic-Carlson, K.; Albertorio, F.; Chilkoti, A.; Cremer, P. S. *Biomacromolecules* **2006**, *7*, 2192.
(20) Cho, Y.; Zhang, Y.; Christensen, T.; Sagle, L. B.; Chilkoti, A.; Cremer, P. S. *J. Phys. Chem. B* **2008**, *112*, 13765.
(21) MacKay, J. A.; Callahan, D. J.; Fitzgerald, K. N.; Chilkoti, A. *Biomacromolecules* **2010**, *11*, 2873.
(22) Meyer, D. E.; Chilkoti, A. *Biomacromolecules* **2002**, *2*, 357.
(23) Frandsen, J. L.; Ghandehari, H. *Chem. Soc. Rev.* **2012**, *41*, 2696.
(24) Kurková, D.; Kríz, J.; Schmidt, P.; Dybal, J.; Rodríguez-Cabello, J. C.; Alonso, M. *Biomacromolecules* **2003**, *4*, 589.
(25) Urry, D. W.; Long, M. M.; Gross, E. *Crit. Rev. Biochem. Mol. Biol.* **1976**, *4*, 1.
(26) Miao, M.; Cirulis, J. T.; Lee, S.; Keeley, F. W. *Biochemistry* **2005**, *44*, 14367.
(27) Platzer, G.; Schedbauer, A.; Chemeli, A.; Ozdowy, P.; Coudevylle, N.; Auer, R.; Kontaxis, G.; Hartl, M.; Miles, A. J.;

11307

dx.doi.org/10.1021/ja4047872 | *J. Am. Chem. Soc.* 2013, 135, 11299−11308

Wallace, B. A.; Glaser, O.; Bister, K.; Konrat, R. *Biochemistry* **2011**, *50*, 6113.

(28) Uversky, V. N. *Protein Sci.* **2002**, *11*, 739.

(29) Tompa, P. *Trends Biochem. Sci.* **2002**, *27*, 527.

(30) Dyson, H. J.; Wright, P. E. *Curr. Opin. Struct. Biol.* **2002**, *12*, 54.

(31) Dreher, M. R.; Elas, M.; Ichikawa, K.; Barth, E. D.; Chilkoti, A.; Rosen, G. M.; Halpern, H. J.; Dewhirst, M. *Med. Phys.* **2004**, *31*, 2755.

(32) Junk, M. J. N.; Li, W.; Schlüter, A. D.; Wegner, G.; Spiess, H. W.; Zhang, A.; Hinderberger, D. *Angew. Chem., Int. Ed.* **2010**, *49*, 5683.

(33) Junk, M. J. N.; Jonas, U.; Hinderberger, D. *Small* **2008**, *4*, 1485.

(34) Kurzbach, D.; Schömer, M.; Wilms, V. S.; Frey, H.; Hinderberger, D. *Macromolecules* **2012**, *45*, 7535.

(35) Atherton, N. M. *Principles of Electron Spin Resonance*; Ellis Horwood: New York, 1993.

(36) Kurzbach, D.; Reh, M. N.; Hinderberger, D. *ChemPhysChem* **2011**, *12*, 3566.

(37) Cimato, A. N.; Piehl, L. L.; Facorro, G. B.; Torti, H. B.; Hager, A. A. *Free Radical Biol. Med.* **2004**, *37*, 2042.

(38) Yamaoka, T.; Tamura, T.; Seto, Y.; Tada, T.; Kunugi, S.; Tirrell, D. A. *Biomacromolecules* **2003**, *4*, 1680.

(39) Meyer, D. E.; Chilkoti, A. *Biomacromolecules* **2004**, *5*, 846.

(40) Kurzbach, D.; Wilms, V. S.; Frey, H.; Hinderberger, D. *ACS Macro Lett.* **2013**, *2*, 128.

(41) Rubinstein, M.; Colby, R. *Polymer Physics*; Oxford University Press: New York, 2004.

(42) Dunker, A. K.; Obradovic, Z. *Nat. Biotechnol.* **2001**, *19*, 805.